01 Aug 2023

Design And Simulation Of A Utility Oilfield Flare In Iraq/Kurdistan Region Using CFD And API-521 Methodology

Ahmed A. Maaroof

Joseph D. Smith
Missouri University of Science and Technology, smithjose@mst.edu

Mohammed H.S. Zangana

Recommended Citation

A. A. Maaroof et al., "Design And Simulation Of A Utility Oilfield Flare In Iraq/Kurdistan Region Using CFD And API-521 Methodology," *Heliyon*, vol. 9, no. 8, article no. e18581, Elsevier, Aug 2023.
The definitive version is available at https://doi.org/10.1016/j.heliyon.2023.e18581

Heliyon 9 (2023) e18581

Contents lists available at ScienceDirect

Heliyon

journal homepage: www.cell.com/heliyon

Design and simulation of a utility oilfield flare in Iraq/Kurdistan region using CFD and API-521 methodology

Ahmed A. Maaroof [a,*], Joseph D. Smith [b], Mohammed H.S. Zangana [a]

[a] Petroleum Engineering Department, Koya University, Koya KOY45 AB64, Kurdistan Region, Iraq
[b] Department of Chemical and Biochemical Engineering, Missouri University of Science and Technology, Rolla, MO, 65409, USA

ARTICLE INFO

Keywords:
Gas flare
CFD
Flare design
CE
DRE
Emissions
Radiation

ABSTRACT

This paper aims at reviewing and analyzing the operation and design of a utility flare in an oilfield in the Iraq/Kurdistan region. The flare supports a gas separation unit that separates 100 MMSCFD of natural gas from other liquid compounds in petroleum refining. The actual flare dimensions are 50 m high and 0.6 m diameter and works in summer where the crosswind speed is 9 m/s and a flow of 1.2 MMSCFD of treated natural gas is flaring through it. At the beginning, the flare design was performed using the API-521 recommended approach based on full operating capacity of the unit and composition of the gas to be flared. The API-521 based design resulted in a flare with a 0.76 m diameter and 48.19 m height. The effects of stack height on heat radiation in case of full capacity firing showed that as the flare height increases from 42.34 m to 133.05 m, the heat radiation decreases from 15.8 kW/mˆ2 to 1.6 kW/mˆ2 within 45.7 m dimeter. Furthermore, the relation between stack height and heat radiation was studied for the actual firing rate 1.2MMSCFD using simulation, where the results showed that as the stack height increasing from 10 m to 50 m the heat radiation decreasing from over 1000 w/mˆ2 to around 150 W/mˆ2. In fact, CFD code C3d was used to analyze flare performance at normal firing condition during summer operation of 1.2 MMSCFD with a flare diameter and height of 50 m and 0.6 m, respectively. The code was able to predict the flame shape and size during actual flare operation. The results of the simulation demonstrated by defining four locations in the domain to measure the average temperatures and emissions, and to calculate the Combustion Efficiency (CE) and Destruction and Removal Efficiency (DRE). These points were 6 m, 8 m, 10 m, 12 m far from the tip on x-axis and at height of 52 m. The results showed that the average temperature at 6 m far from the flare is 658 K and it decreasing to 490 K at 12 m away from the tip. The CO and CO2 also decreased from 7.27E-5 and 0.033 mass% to 4.53E-6 and 0.027 mass%, respectively. Generally, soot formation was low but at points 8 m and 10 m from the tip the soot formation was considerably lower, respectively at 6.16E-5 and 8.71E-5 mass%. The emissions of C1, C2, C3 and C6+ were measured at 7.46E-9, 5.39E-9, 5.13E-9 and 4.35E-9 mass% at 6 m away from the tip. The emissions increased slightly at 8 m and 10 m from the tip but at 12 m they were observed to decrease. The flare CE and DRE were estimated to be 98% and 100%, respectively. Analysis results confirmed that the flare design was safe and the flare operation was highly efficient with very little smoke produced as indicated by the predicted CE and DRE.

* Corresponding author.
E-mail addresses: ahmed.maaroof@koyauniversity.org (A.A. Maaroof), smithjose@umsystem.edu (J.D. Smith).

https://doi.org/10.1016/j.heliyon.2023.e18581
Received 25 April 2023; Received in revised form 21 June 2023; Accepted 21 July 2023
Available online 27 July 2023

1. Introduction

Generally, a gas flare is a combustion device used for burning gases that cannot be stored or processed due to economical, technical or safety reasons [1]. Flares are used in petroleum industry for extraction of oil or gas from wells in both offshore and onshore applications, and in refineries. Additionally, gas flares are also used in other industries to burn waste gas from coal-gasification, sewage digesters, and ammonia fertilizer plant [2].

Nowadays, gas flaring is considered a significant challenge climate change because of the carbon emissions produced by the flare [3,4]. Gas flaring affects local populations by producing undesirable by-products including noise, smoke, thermal radiation, SOx, NOx, Soot, CO and CO_2. Proper flare design and operation can minimize these impacts. Gas flaring volume is directly related to the level of oil production. Fig. 1 shows the relation between oil production and gas flaring worldwide. Fig. 2 compares global gas flaring volume for the top 10 countries between 2012 and 2022.

Table 1 and Fig. 3 show the effect of increasing oil production in Iraq on flaring volume and intensity. As shown, the flaring volume and intensity is almost stable even with slightly decreasing oil production in 2020 and 2021. This can be explained due to improper flare operation and design in some locations in the oil field in Iraq.

Flare performance can be quantified using Combustion Efficiency (CE) and Destruction and Removal Efficiency (DRE) [6–11]. The DRE measures the amount of destroyed original fuel converted to CO_2 and CO, while CE measures how much of the original fuel burns completely to produce CO_2 & H_2O. In flare design, both CE and DRE need to be considered [12–15]. Studies have shown that a good DRE can be obtained if the flame burns in a stable fashion [12,16].

Moreover, the relationship between gas heating value and tip exit velocity is a factor that affects flame stability. Flares generally generate emissions when they are unstable (e.g., near the point of blowing out) [17,18]. Other parameters affecting flare operation and combustion efficiency is flame lift-off which occurs when the flow velocity at the tip (exit velocity) is too fast and exceeds the burning velocity of the flare gas. To avoid the flame's lift off, the USEPA has suggested that the flare tip velocity should be less than the maximum allowable flare tip velocity determined by the flare tip diameter, the density of the flared vent gas and the air and combustion zone gas composition. The key factors important in determining the flare flame stability includes flame speed, flammability limits and ignition temperature [18,19]. The ambient wind velocity also affects the flame size and shape and can affect the heat radiation from the flame [19,20].

In flare design, the following factors are important to achieve best performance and meet regulations; flow rate, gas composition, gas temperature, gas pressure, utility cost and availability, environmental requirements, safety requirements, and social requirements [2]. Furthermore, the design should consider the following requirements; first, flares should install at least as high as any platform within 150 m horizontally, and not less than 15 m high. Second, the base of flares should install at least 60 m away from any source of flammable hydrocarbons. Third, the location & height of flares should meet all applicable standards for atmospheric pollution & noise. Fourth, flare spacing & elevation should be such that permissible radiation heat intensities for personnel at grade be less than the allowable limit (1.6 kW/m^2) under condition of maximum heat release. Finally, the minimum distance from the flare stack base to nearby property line should be 60 m [16,21].

During operation, plume forms from the visible flame and travels downwind of the flare stack. As a result of temperature differences between the surrounding air and flare plume, buoyance will lead to rise the plume and expand it as it mixes with cooler air in the surroundings. Generally, pollutants and heat will disperse into the surrounding atmosphere as the plumes rise and expand; therefore, it has been observed that pollutants and heat will travel more until they reach the ground level. In general, momentum and buoyancy are the main two factors that control plume rise [22]. Flare height must be calculated to ensure that unburned toxics will not exceed the limit of safe dispersion (ground level concentration) [16]. This paper aims at evaluating the design and operation of a utility flare that operate in Iraq/Kurdistan region to burn 1.2 MMSCFD in summer. This work will check the hydraulic limits of the flare using API-521 design approach and maximum gas flow rate (100MMSCFD) passing to the flare. Furthermore, this paper will evaluate the safety limits and performance using CFD code C3d. According to hypothesis, safety factor should increase when the flare height increases due to decreasing amount of heat radiation and emissions to ground. The flare performance will be evaluated depending on the CE and DRE results. High DRE is expected to obtain if the difference in the concentrations of the fuel in the plume and the gas being sent to the flare

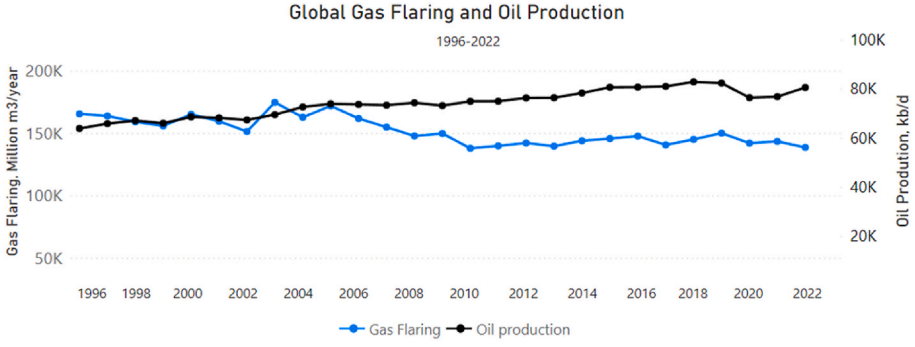

Fig. 1. World-wide flaring volume (million m^3/year) and oil production (thousand barrels per day) (1996–2022) [55].

was high. Moreover, high CE is expected to observe as a result of smokeless operation, and low emissions of carbon monoxide and soot formation. The following parts will discuss first the design and then evaluate of the flare operation.

2. Case study

Data of a utility flare operating in an oil field in Kurdistan region of Iraq has been collected and used in this study. The case study flare is designed for a maximum capacity of 100 MMSCFD (capacity of the gas separation unit). The flare height and diameter are 50 m and 0.61 m (24″), respectively (see Fig. 4). The gas composition sent to flare shown in Table 2, and the actual flame size and shape during summer is shown in Fig. 4. Figs. 5 and 6 are graphical ways to design the flare considering the wind effect on the flame.

The flare design was performed using API-521 recommended practice for determining the maximum capacity of the flare. In the following parts, the flare design will be carried out based on maximum capacity 100 MMSCFD to check the actual flare hydraulic limits if its capable of burning the full plant capacity in case of failure.

2.1. Flare design using API-521 recommended practice

The flare design using the equation and method provided by API-521 determines the flare height and diameter. At the beginning, the flare gas composition (mole basis) was converted to mass basis (see Table 2). After that, the gas average molecular weight, density and lower heating value have been calculated (see Table 3).

The flare gas mass flow rate was obtained through the following steps.

Flow rate (Max Capacity) = 100 MMscfd = 118,000 m^3/h.

(1 **MMscfd** = 1180 M^3/hr).

Density, $\rho = P/\left(\frac{R}{M} * T\right) = \frac{101325}{\frac{8314.3}{19.25} * 300} \approx 0.782$ kg/m^3

$$Mass\ Flow\ Rate\ \left(\frac{kg}{hr}\right) = Flow\ rate\ \left(\frac{m^3}{hr}\right) x\ density\ \left(\frac{kg}{m^3}\right)$$

$$Mass\ Flow\ Rate\ \left(\frac{kg}{hr}\right) = 118,000\left(\frac{m^3}{hr}\right)\ x\ 0.782\left(\frac{kg}{m^3}\right) = 92,276\frac{kg}{hr}\ \left(25.63\ \frac{kg}{s}\right)$$

The required information for the flare design is listed in Table 4.

The results of the calculations are listed in Table 5. These results have been obtained using the equations and charts in Table 6.

Fig. 7 shows the flare dimensions obtained using API-521 method. The flare height was 48.2 m with a diameter of 0.76 m. These dimensions are near to the flare dimensions in the plant. The reason for using slightly smaller diameter is to increase the gas velocity injected since at normal operation less than the maximum capacity is sent to the flare.

2.1.1. Flare performance

The LHV of gas mixture is 46266 kJ/kg on volume basis which equals to

$$LHV = 46,266\ \left(\frac{kJ}{kg}\right)\ x\ 0.782\ \left(\frac{kg}{m^3}\right) = 36180\ \left(\frac{kJ}{m^3}\right) = 971\ \left(\frac{Btu}{ft^3}\right)$$

The Heating value of the gas 971 $\left(\frac{Btu}{ft^3}\right)$ is greater than the recommended minimum of 300 $\left(\frac{Btu}{ft^3}\right)$ for efficient combustion, which mean it can combust according to EPA regulation and guidelines.

2.1.2. Combustion stability

The flare gas tip velocity is (236.22 ft/s) with as heating value of 971 Btu/ft^3, the combustion should be stable above the flare tip because the velocity and heating value are in the recommended range (gas tip velocity < 1000 ft/s, heating value > 800 Btu/ft^3).

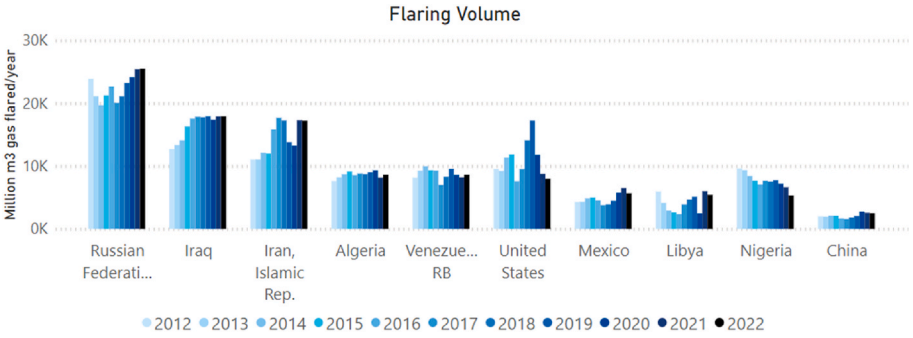

Fig. 2. Top 10 flaring countries by volume flared (2012–2022) [5].

2.1.3. Combustion efficiency

The flare combustion efficiency at max firing capacity is expected to be > 98% based on the equation and chart below (see Fig. 8).

$$\frac{Heating\ value}{Minimum\ heating\ vlaue} = \frac{971}{300} = 3.23$$

2.1.4. Wake stabilized

Wake stabilized analysis for the full capacity flare operation is shown below.

$$\textbf{wind air momentum} = \rho_a U_w^2 = \mathbf{1.225\ x\ (9)^2 = 99.225} \frac{kg}{m.s^2}$$

$$\textbf{Flare gas momentum} = \rho_f U_f^2 = \mathbf{0.782\ x\ (72)^2 = 4043.52} \frac{kg}{m.s^2}$$

Since the momentum of exiting flare gas is higher than the cross flowing air, no effects are expecting during maximum flaring.

2.1.5. Smokeless operation

For this design, burning flare gas is expecting to generate some smoke as it contains propane (C_3 with C/H = 0.375) and Hexane (C_6^+ with C/H = 0.43) which have C/H ratios higher than the recommended values of 0.35 (see Table 7). Therefore, as recommends to using steam assist or air assist to achieve smokeless operation. For Iraq, it is recommended that an air-assisted flare to enhance mixing due to water shortage.).

2.1.6. Effect of mach number on diameter and height of stack

According to API-521 standard, the conservative Mach number is between 0.2 and 0.5. By repeating the design steps for the same gas composition and data input but using a different Mach number results in decreasing stack height and increasing the tip velocity (see Table 8, Figs. 9 and 10).

2.1.7. Effect of mach number on diameter and height of stack

Fig. 11 and Table 9 show the effect of K (allowable radiation limits) on D (distance from center of flame to surface objects). This study carried out to show the effect of changing the flare height on amount of heat radiation to ground. This analysis depends on assuming D = h (height of the stack).

Comparing stack height (133.05 m) with the estimated stack height (42.34 m), the former has less radiation safety issue in the workplace. However, the cost for the taller stack is higher than the API design. In general, the best design will consider worker's safety first. According to API-521 recommendations, a flare stack height of 67.05 (k = 6.3 kW/m^2) is acceptable since plant personnel can work around it for up to 1 min. For more safety a higher sack should be considered.

2.3. CFD analysis of the flare operation

After designing the flare using API-521 approach, CFD code C3d versions 12.21.21 has been used to analysis the flare operation at normal firing rate 1.2MMSCFD during summer (wind speed 9 m/s) and using the actual flare dimensions 50 m height and 0.61 m diameter. In this simulation, the gas composition, density, wind speed and temperature used in the design of the flare has been used also in the simulation.

2.3.1. C3D code (background)

Generally, C3d is a computational fluid dynamic (CFD) and heat transfer computer code aimed at solving a wide range of heat transfer and fluid mechanics problems in cases involving fires and flares. The code includes several optional sub models that help simulate radiation heat transfer, deposition and aerosol transport, material decomposition, chemical reactions, and combustion [25].

The C3d code has been used in several previous works [26–28]. This code is based on a CFD tool originally known as ISIS-3d, and it has been validated and used for simulating pool fires to investigate thermal performance of nuclear transport packages [29–31]. Originally, the code was developed at Sandia National Laboratory, and has been commercialized into a new CFD tool known as C3d to

Table 1
Iraq flaring volume, Flare intensity and oil production (2016–2022) [5].

Years	Flaring Volume (Million m^3/year)	Flare Intensity (m^3 per barrel of oil produced)	Oil Production (1000 barrels per day)
2016	17,551.52	10.82	4443.52
2017	17,843.04	10.98	4454.69
2018	17,767.14	10.55	4612.70
2019	17,914.22	10.35	4740.62
2020	17,373.79	11.64	4088.22
2021	17,891.97	12.00	4084.82
2022	17,902.88	10.96	4474.17

be used for analyzing the performance of large gas flare. In fact, C3d has been used previously for evaluating the performance of air assisted flares, non-assisted (utility) flares, and large multipoint ground flares [26,32] with the combustion model expanded and approved for application and testing of typical flare gas (methane, propane, ethylene, xylene, ethane and propylene). Furthermore, C3d has been used for predicting flame shape and size, estimating the potential for smoking ignition behavior, and estimating the radiation flux from the flame to surrounding objects.

I code has also been used to analyze multi-point ground flares and air flow through the surrounding wind fence, and the resulting flame shape and height during maximum firing conditions. Also, the code has helped to evaluate the spacing between flare tips and rows to ensure adequate air flow to individual burners during operation to avoid smoking during maximum relief conditions [33]. Moreover, the code has been used to study the impact of using a continues pilot compared to a discrete ignition system, whereas various ignition scenarios considering instantaneous ignition compared to delayed ignition [32].

2.3.2. Using LES versusu RANS CFD

Studies shown that the traditional CFD simulation tools which use the Reynolds-Averaged Navier-Stock (RANS) approximations may not compute accurately the flare combustion efficiency. This is because of large-scale mixing resulting from vertical coherent structures in the flames are not easily reduced to a steady state condition provided by a typical RANS. Furthermore, in RANS, unsteady information (i.e., flame shape & instantaneous mixing) cannot be properly captured by time averaging the equations.

Industrial flares operate in turbulent flow conditions, which include large disparity time and length scales. The smallest of these scales is set by viscosity and the biggest is on the order of flare tip diameter. Generally, the combustion is limited by mixing rates due to non-premixed combustion. There are numerous centrally reaction steps with hundreds of species with a wide range of reaction time scales involved in the detailed kinetic mechanism of chemical reactions. Both radiative and convective heat transfer accompany in the exothermic nature of the chemical reactions. These processes are closely coupled; for instance, the chemical reactions are affected by turbulent mixing air and combustion gas. The chemical reactions change the density and consequently the mixing intensity through turbulence. This occurs because the gas temperature changes with the chemical reactions as heat is generated. Resolving all the time and length scales in practical turbulent combustion applications is very difficult and mostly not possible even with supercomputers. Alternatively, capturing important features of the flame can be done through resolving large time and length scales, responsible for the controlling dynamics, and using subgrid scale models for more homogenous smaller scales. It has been observed that the Large Eddy Simulation (LES) approach can more accurately simulate transient flare gas combustion compared to an RANS approach [34–38].

2.3.3. Computational domain and boundary conditions

The computational domain size used in this work was 70 m high, 45 m in length and 40 m in width. The height of the domain (z-axis) started from – 0.1 to 0 to specify ground for the flare, then from zero to 70 m. The domain length (x-axis) started from – 5 m to 40 m. Finally, the domain width (y-axis) started from – 20 to 20. Starting the x and y domains at – 5 and −20 set the center of the flare so the cross wind would blow from the x-axis. In this simualtion, the flare height and diameter were 50 m and 0.61 m, respectively. Fig. 12 shows the flare location in the domain and the mesh size. The total number of hexahedral cells were 1,850,625 (141 × 125× 105), and was finer near to flare tip to capture the flame shape and transient nature correctly.

Fig. 13 shows a mesh inpependence study considering soot formation (ppmv) in the plume for three different mesh sizes. For this study, a probe was located at 6 m, 8 m, 10 m and 12 m (on x-axis), 0 m (on y-axis) and 52 m (on z-axis) in the domain to capture the soot in the plume. According to the results, with fewer cells the predicted soot (C_{20}) formation was higher than with more cells. To ensure best results, the most refined mesh (1,850,625) was used for all work reported in this paper.

The boundary conditions used in this work included: constant 9 m/s cross wind at 300 K blowing from the x-axis to the flare and

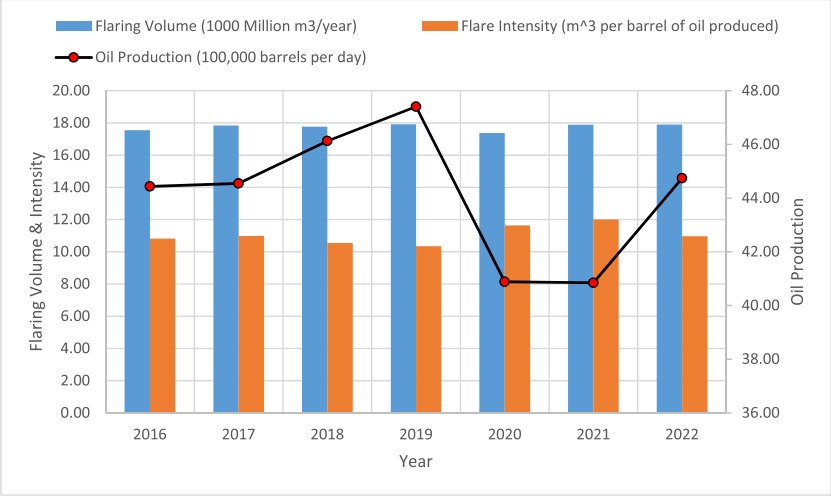

Fig. 3. The correlation between flaring intensity, flaring volume and oil production [5].

Fig. 4. Case study flare operation at 1.2MMSCFD of gas injection.

Table 2
Case study Gas composition.

Basis = 100 kg mol/h					
Components	Mole (%)	Kg mole	MWt	Kg.	Mass (%)
C1	83.34	83.34	16	1333.44	0.693
C2	9.501	9.501	30	285.03	0.148
C3	3.391	3.391	44	149.204	0.078
C6+	0.232	0.232	86	19.952	0.010
CO2	1.713	1.713	44	75.372	0.039
H2S	1.816	1.816	34	61.744	0.032
N2	0.007	0.007	28	0.196	0.000
Total	100	100.00		1925	1

Average molecular weight $= \frac{Total\ mass}{Total\ mole} = \frac{1925\ kg/hr}{100\ kg\ mole/hr} = 19.25 \frac{kg}{kg\ mole}$.

with hydrostatics pressure defined across the domain. Three 1-d sub grids were defined for the ground, flare wall and flare tip. In the first sub grid, dry sand was selected as the material for the ground of flare. In the second sub grid, carbon steel was selected as the material for the stack. Finally, in the last sub grid, the mass flux and temperature of the gas through the flare was defined as 1.08 kg/m^2.s (equal to 1.2 MMSCFD) and 300 K, with the flare exit as a 3-D pressure.

2.3.4. Physical model

In this simulation, the LES turbulence model was used to simulate fluid flow. Radiation effects were included in the energy equation. To keep monitoring the fuel distribution and concentration, soot, intermediate species, and products of combustion (H_2O and CO_2), individual species equations were also solved. The combustion model used for providing the sink and source terms for the species equations as a function of local gas temperature, species concentrations and turbulent diffusivity.

The code predicted the flame emissivity using a series of models as a function of soot volume fraction, molecular gas composition, flame size, flame shape and combustion effluent temperature profile. These variables depend on solutions of the momentum, mass, species, and energy equations. In this simulation, radiation transport model used for predicting the radiation flux from the flame to

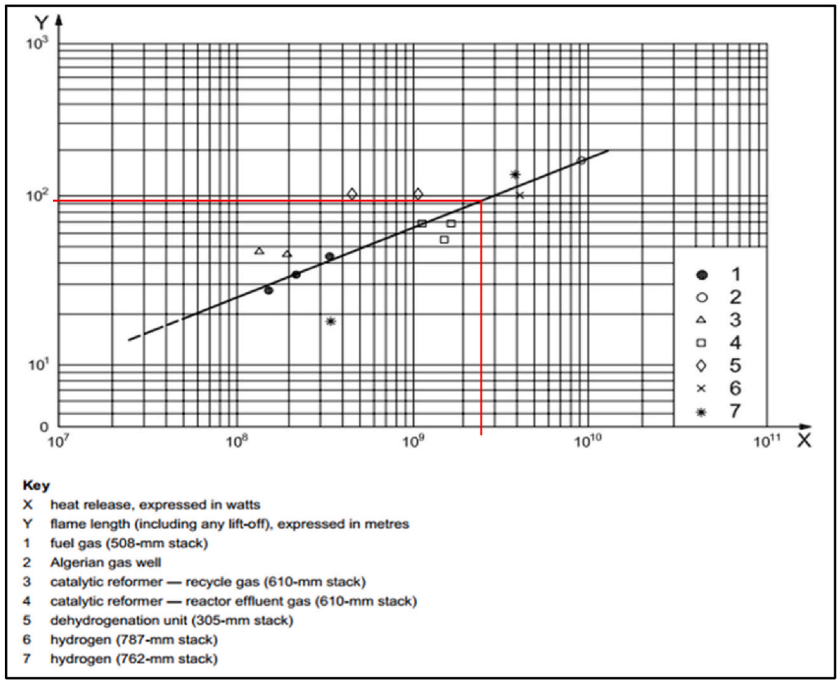

Fig. 5. Flame length versus heat released [20].

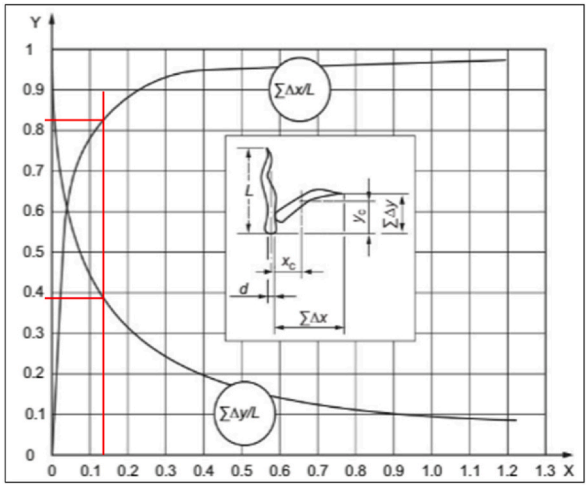

Fig. 6. Approximate wind distortion due to lateral wind on jet from flame stack [16].

Table 3
Heating value calculations.

Components	Mass fraction	LHV (kJ/kg)	LHV x Mass fraction (kJ/kg)
C_1	0.693	50,048	34,669.17
C_2	0.148	47,611	7049.87
C_3	0.078	46,330	3591.09
C_6+	0.010	45,099	467.45
CO_2	0.039	–	
H_2S	0.032	15,223.67	488.31
N_2	0.000	–	
Total	1		**46,266**

Table 4
Design data.

Input Data		
Wind velocity	9	m/s
R (reference point)	45.7	m
Mach number (0.2–0.5)	0.2	dimensionless
Mass flow rate	25.63	Kg/s.
Molecular weight	19.25	Kg/kmole
Temperature of gas at tip	300	K
LHV	46266	kJ/kg
γ (cp/cv)	1	dimensionless
Pressure	101,325	Pa
Z (compressibility)	1	dimensionless
K max (allowable radiation)	6.3	kW/m^2
fraction of heat transmitted (τ)	1	dimensionless
fraction of heat radiated (E)	0.3	dimensionless

Table 5
Design results.

Output Data	
Tip Velocity (m/s)	72
Tip Area (m^2)	0.45
Tip Diameter (m)	0.76
Stack Height (m)	48.2
Heat Liberated (kW)	1,185,898
Flame length	95
Distance from the center of flame to ground (m)	67.06

Table 6
Equations used in the design [16].

Tip sizing		
Speed of Sound (c)	$c = \sqrt{\frac{\gamma RT}{M}}$	T = Temperature M = Molecular weight R = gas constant γ (cp/cv)
Tip velocity	(V_{tip}) = c * Mach	
Tip area	$A = \frac{\dot{m}}{\rho v}$	$\dot{m}$ = gas mass flow rate ρ = *gas density* v = *gas velocity*
Tip diameter	$d = \sqrt{\frac{4 * A}{\pi}}$	A = Tip Area
Flame length		
Heat liberated	Q = *Flow* * *LHV*	
Flame Length	Figs. 5 and 6	
Wind effects (flame distortion)		
Distance	$D = \sqrt{\frac{\tau EQ}{4\pi K}}$	
Stack height	$\frac{U_\infty}{U_{tip}}$ r' = r – x_c h'^{2} = D^2 - r'^{2} h = h' – yc	U_∞ = *wind velocity* U_{tip} = *Tip Velocity*

external ground, as well as providing sink and source terms for the energy equation to predict the flame temperature distribution.

2.3.5. Chemical and soot model

The rate of combustion equations is defined by a combination of Arrhenius & Eddy breakup reaction time scales.

$$t_{total} = t_{reaction} + t_{turb} = \left(\frac{1}{A_k T^b e^{-\left(\frac{T_A}{T}\right)}}\right) + \frac{C_{eb} dx^2}{\varepsilon_{diff}} \quad (1)$$

A_k is the pre-exponential coefficient, T is the local gas temperature, b is a global exponent, T_A is activation temperature, C_{eb} is the eddy breakup scaling factor, dx is the characteristic cell size, ε_{diff} is the eddy diffusivity from LES module, t_{turb} is the turbulence time

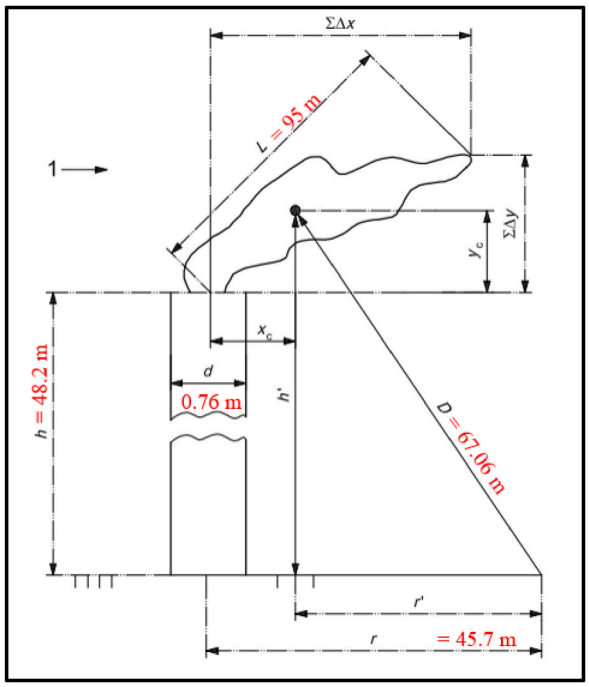

Fig. 7. Flare stack dimensional reference [16].

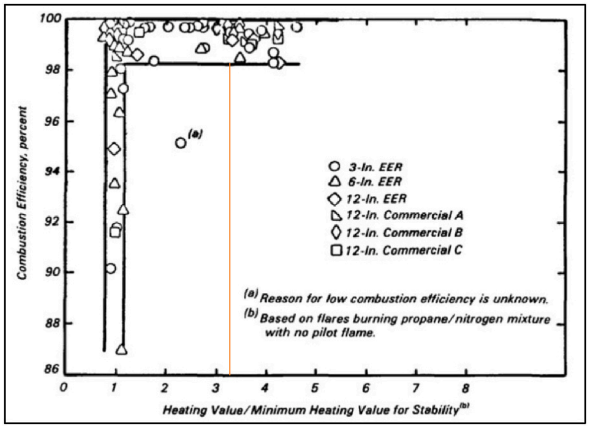

Fig. 8. Heating value/ minimum heating value versus CE [23,24].

Table 7
C/H ratio of the gas mixture.

Components	C/H	Mole %	Mass Fraction
CH_4	0.25	83.34	0.69
C_2H_6	0.33	9.50	0.15
C_3H_8	0.375	3.39	0.08
C_6H_{14}	0.428	0.23	0.01
CO_2	–	1.71	0.04
H_2S	–	1.82	0.03
N_2	–	0.01	0.0001
Total	1.00	100	1

Table 8
Flare dimensions and tip velocity versus mach number.

Mach	Stack Height (h) m	Stack Diameter (d) m	Stack Tip velocity (m/s)	Stack Tip area (m^2)
0.2	48.19	0.76	72	0.46
0.3	43.34	0.62	108	0.30
0.4	39.58	0.54	144	0.54
0.5	37.37	0.48	180	0.48

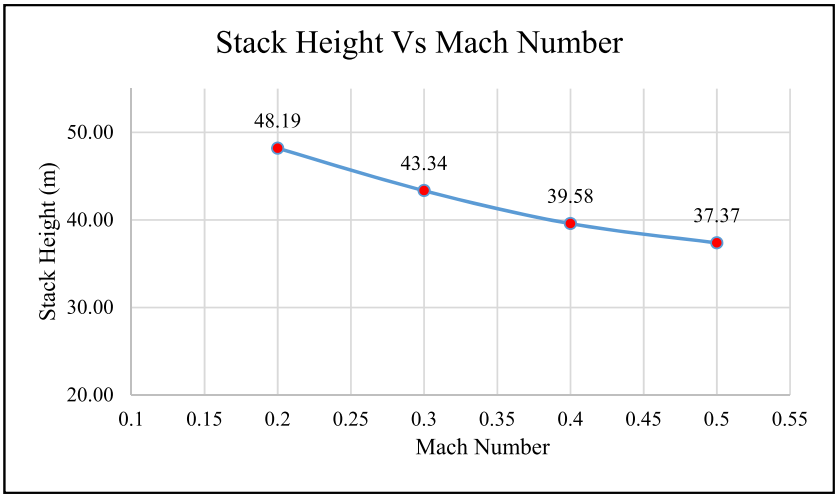

Fig. 9. Stack height at different mach numbers number (0.2, 0.3, 0.4 and 0.5).

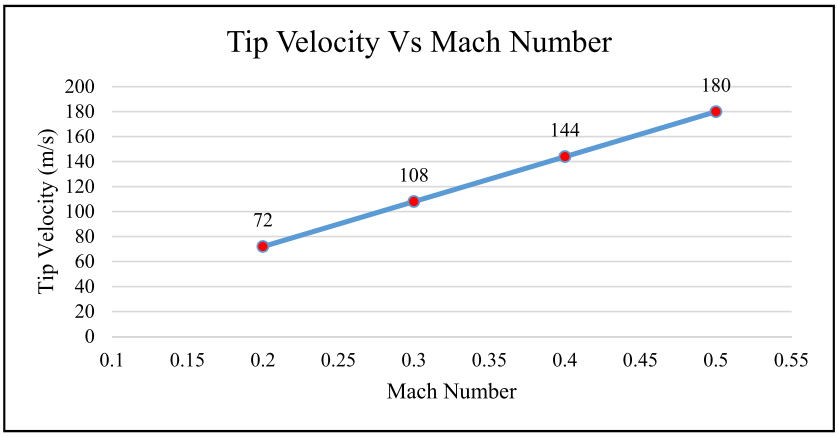

Fig. 10. Tip exit velocity at different mach numbers (0.2, 0.3, 0.4 and 0.5).

scale [25].

The combustion chemistry includes primary fuel breakdown reactions (incomplete combustion) that produce intermediate combustion products (C_2H_2, H_2, CH_4, Soot, and CO). Next, the reactions include burning the intermediate products and produce soot. Furthermore, reforming reactions with OH radicals are included, and the oxidizing species are simplified as water vapor. Equilibrium reactions between methane, acetylene, hydrogen, hydrogen sulfide and sulfur are included to allow to form soot [25].

The primary fuel breakdown reactions in this study are shown below:

CH_4 + O_2→ H2 + CO + H2O C1 Breakdown

C2H6 + O2→ 2.5H2O + 0.5C2H2 + CO C2 Breakdown

C3H8 + 1.5O2→ C2H2 + 2H2O + CO + H2 C3 Breakdown

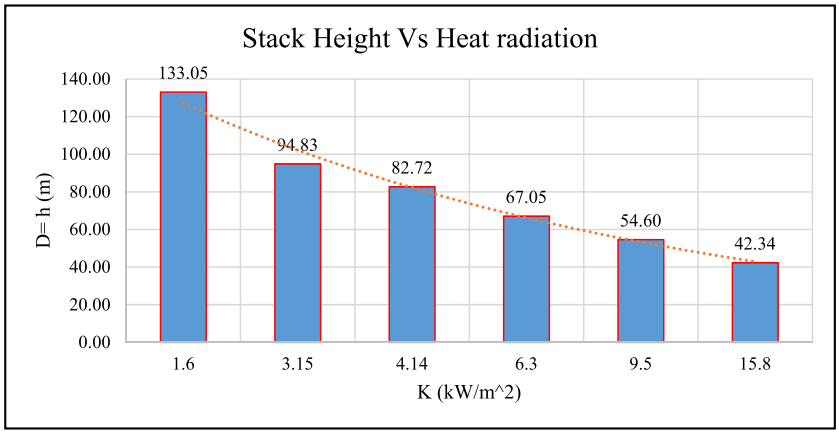

Fig. 11. Flare height versus heat radiation.

Table 9
Flare height and heat radiation.

D = h (m)	K (kW/m^2)	API-521 recommendation
133.05	1.6	Personnel, continuous
94.83	3.15	
82.72	4.14	Personnel, few minutes
67.05	6.3	Personnel, 1 min
54.60	9.5	Personnel, a few seconds
42.34	15.8	Equipment only

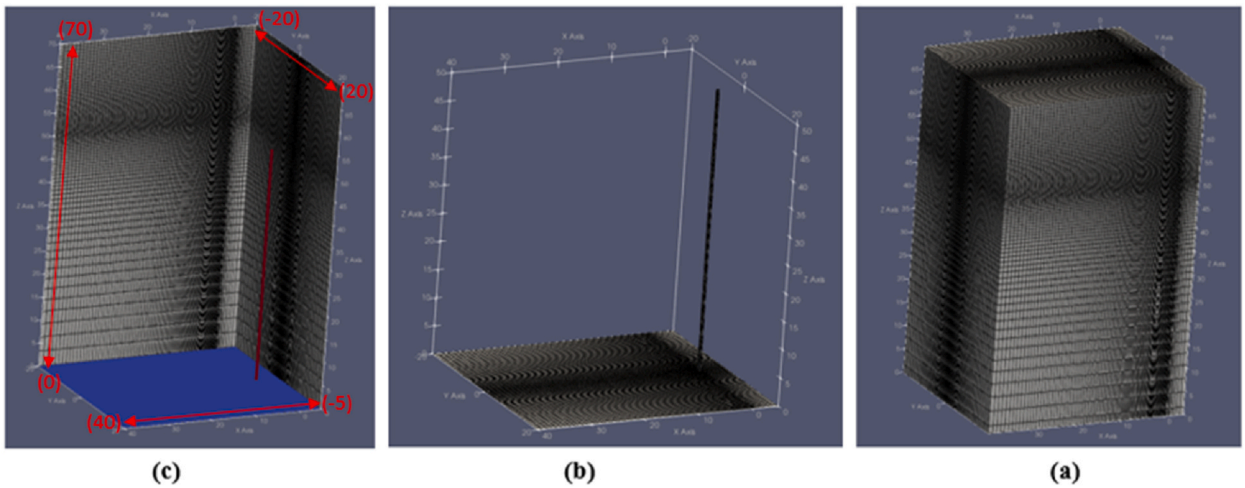

Fig. 12. (a) Domain size and mesh, (b) Flare and ground mesh (c) Flare surrounding mesh.

C6H14 + 3.5O2→ 5H2O + 2C2H2 + 2CO C6+ Breakdown

H2S + O2– > SO2 +H2 H2S Breakdown

The secondary reactions of the gas are shown below:

H2 + 0.5 O2→ H2O H2 combustion

C2H2 + 0.8 O2→ 1.6 CO + H2 + 0.02C20 (soot) nucleation soot formation

C2H2 + 0.01C20→ H2 + 0.11C2 soot growth by acetylene addition

CO + 0.5 O2→ CO2 + H2O CO combustion

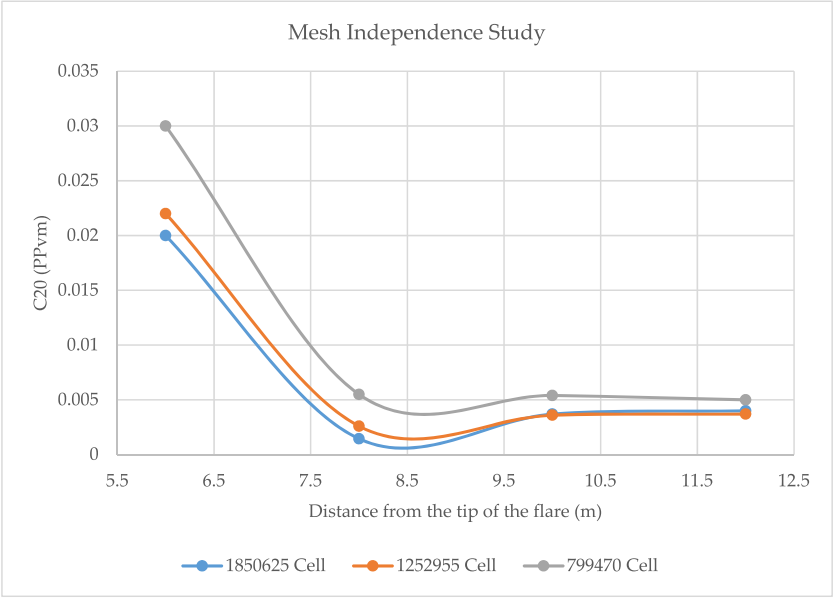

Fig. 13. Mesh Independence study for Soot in the Plume.

C20 + 10 O2→ 20 CO soot combustion

C2H2 + 3H2→ 2 CH4 acetylene decomposition

CH4 + CH4→ C2H2 + 3H2 acetylene formation

O.5 S2 + H2→ H2S sulfur reduction to hydrogen sulfide

H2S–> 1.5 S2 + H2 hydrogen sulfide decomposition

H2S + 0.5 〖SO〗_2→ 0.75 S_2 + H_2 O elemental sulfur formation

The reforming reactions are showing below:

C_20 + 20 H_2 O–> 20 CO + 20 H_2 soot steam reforming.

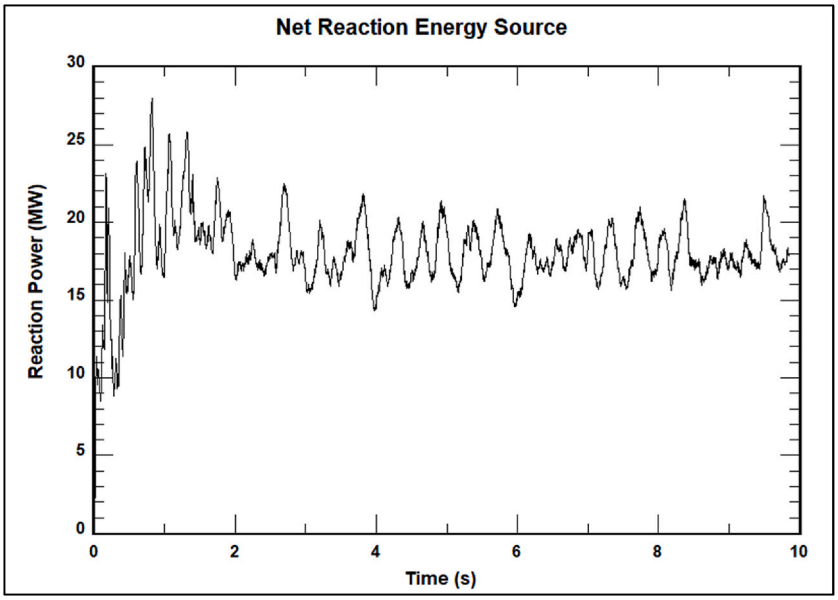

Fig. 14. Net reaction energy source for simulations.

$0.75S_2 + H_2O- > H_2S + 0.5\ SO_2$ sulfur steam reforming

For these reactions, a global Arrhenius rate mode is used. The consumption of soot, fuel and intermediate species are described by:

$$\frac{df_{R_i}}{dt} = -C\left[\prod_i^N f^{p_{A_i}}\right] T^b e^{-(T_A/T)} \tag{2}$$

where N = number of reactants, f_{R_i} = moles of each reactant, i and C = pre-exponential coefficient, T_A = effective activation temperature and b = temperature exponent.

2.3.6. Post processing and transient calculation

At the beginning, the simulation run for 10 timesteps to calibrate the gas mass flow rate injected through the flare 0.31 kg/s which is equivalent to 1.2 MMSCFD (Case study flow rate). After this step, the simulation timesteps and time set to 10000 step and 10 s, respectively to allow the process to stabilize. The net reaction energy source (Fig. 14) shows the simulation reach stability after 3–4 s.

3. Results

Paraview (version 5.10.0) was used to visualize the flame and extract results of combustion products, temperature, velocity of the flame and other properties.

3.1. Flame shape, size and prodcuts of combsution

The C3d code was able to give a good estimation of the flame shape and size compared to the real flare (see Fig. 15).

Fig. 16 shows the flame temperature, soot concentration (ppmv) and methane concentration (mass %) in the plume.

These figures show that the temperature inside the flame is around 2000 K and its decreasing due to cooling by cross wind. Furthermore, the soot formation is significantly low approximately 0.6 ppmv, and methane concertation is about 0.1 mass% inside the flame. Moreover, Fig. 17 shows the mass fraction of oxygen, carbon monoxide and carbon dioxide in the plume.

According to Fig. 17 (a), oxygen concentration around the flame is higher than the center of the flame to maintain the complete combustion. The complete combustion of the flame can be observed from Fig. 17 (b) and (c) where the carbon monoxide concertation is low compared to carbon dioxide concertation. Due to the cross wind effect, the oxygen concentration increasing, the carbon dioxide decreasing at the end of the flame as a result of changing in the stoichiometric ratio lead to producing very little smoke (see Fig. 16 b).

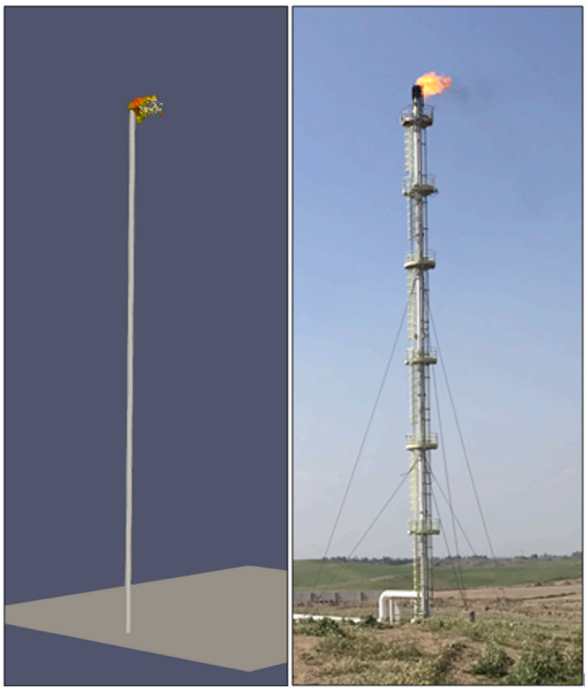

Fig. 15. Flare shape and size predicted by the C3d code and the real flare.

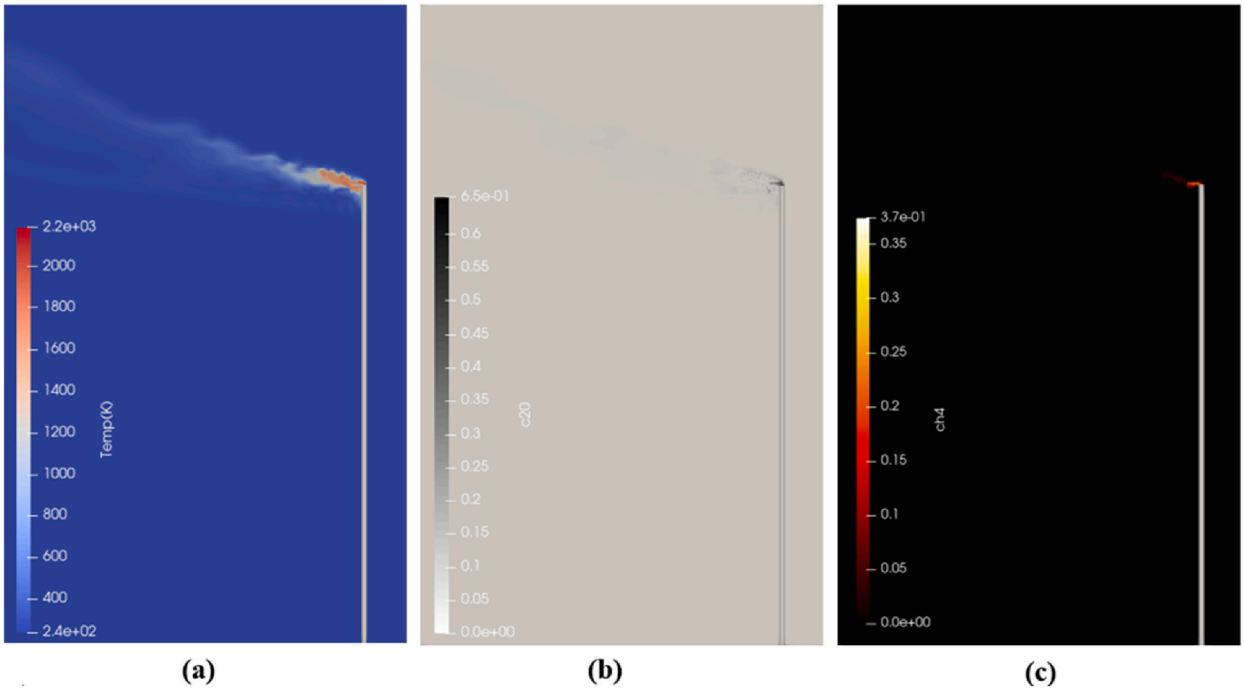

Fig. 16. Products of combustion; (a) flame temperature (K), (b) soot (ppmv), and (c) CH4 (mass%).

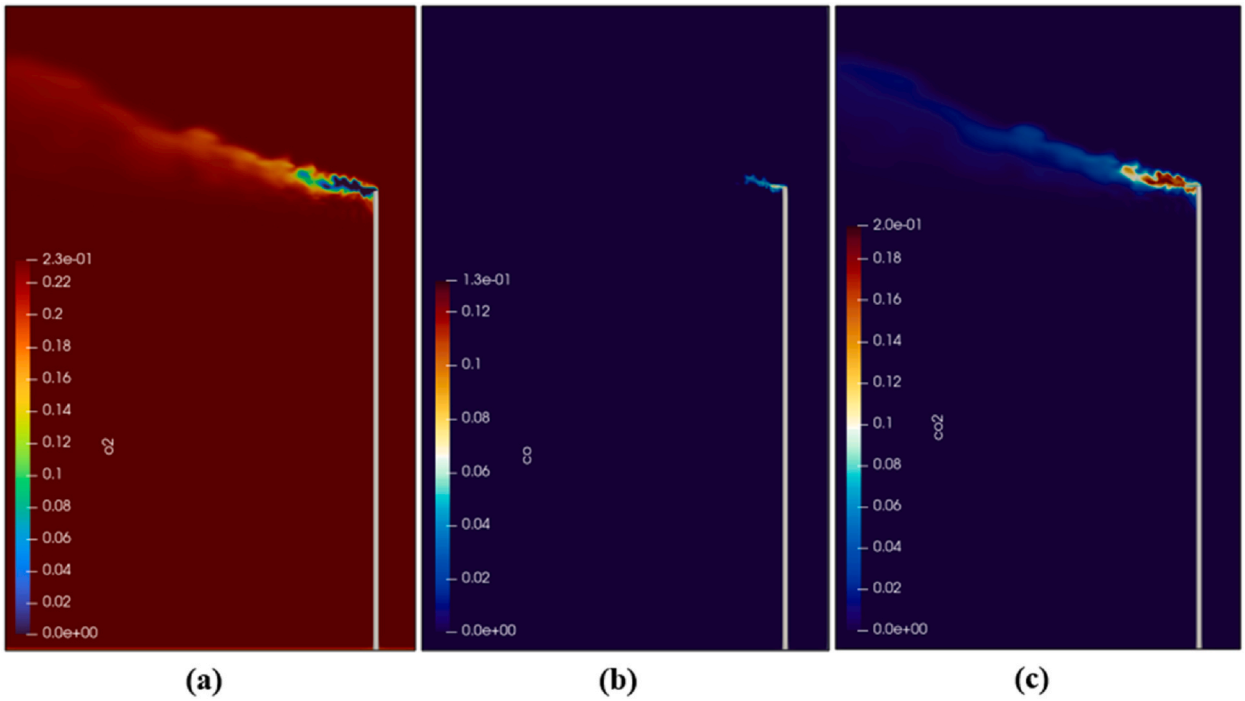

Fig. 17. Products of combustion; (a) O2 (mass %), (b) CO (mass%), and (c) CO2 (mass%).

3.2. Flare stack height effect and ground heat

Three different stack elevations have been studied to show the effect of changing flame distance from ground on amount of heat released to the ground. Fig. 18 shows three stack elevations (10 m, 30 m and 50 m) and ground heat (W/mˆ2) due to the distance from

the flame.

These figures show that the real flare height 50 m (Fig. 18 c) has very low heat radiation to the ground compared to 10 m stack height (Fig. 18 a) with approximately 150 W/mˆ2 and over 1000 W/mˆ2 respectively. This prove that the case study flare considered the safety requirements for flare operation in the area near to the flare.

3.3. Cross wind effect and flare flame

The effect of cross wind speed on flare operation has been studied by considering three scenarios for cross wind speeds; 5 m/s, 9 m/s and 14 m/s. Fig. 19 show the flame shape as a result of changing cross wind speed from 5 m/s to 14 m/s. According to these figures, as the wind speed increases to 14 m/s, the probability of wake stabilizer increases. Moreover, as the wind speed increases, the flame cool faster and increase chances for soot formation and flame shut down. The wind speed of the case study flare (9 m/s) is acceptable with flare firing rate (1.2MMSCFD) as there is less wake stabilizing compared to 14 m/s. However, when comparing 9 m/s with 5 m/s, it's clear that less firing rate can be applied in this case to maintain the flame.

3.4. Combustion efficiency (CE) and destruction and removal efficiency (DRE)

The combustion products and temperature were calculated using probe function in Paraview. The probe radius was set to 0.25 m and located at four different locations in the domain: 6 m, 8 m, 10 m and 12 m (on the x-axis) away from the stack, and 52 m height (on z-axis) to capture combustion products and temperature. At each point, 10 data points were measured and the average calculated (see Table 10 and Table 11). The locations of the probes are shown in Fig. 20.

The output from the code includes the mass fraction of all combustion products except of Soot where it is in ppmv. To convert soot concentration to mass fraction, code output in ppmv is divided as ppmv/10,000 and multiplying it by molecular weight of C_{20} (240 g/mol).

According to these data, the temperature is decreasing from around 650 K at location near to the tip of the flame to 490 K at 12 m away from the flame. This can be explained due to the effect of cooling by cross wind blowing toward the flare from a side. As explained before there is a soot formation but it is low as the carbon monoxide consternation. Comparing carbon dioxide concentration to carbon monoxide concentration, it's clear that the combustion is compete inside the flame.

To evaluate the performance of the flare CE and DRE have been calculated using the following equations:

$$\%CE = \frac{Co2}{Co2 + Co + C1 + C2 + C3 + C_6^+ + Soot} \tag{3}$$

$$\%\mathrm{DRE} = 1 - \frac{\mathrm{C1} + \mathrm{C2} + \mathrm{C3} + \mathrm{C}_6^+ \text{ (Mass \% in the plume)}}{\mathrm{C1} + \mathrm{C2} + \mathrm{C3} + \mathrm{C}_6^+ \text{ (Mass \% in the original fuel)}} \tag{4}$$

$$\%\mathrm{DRE}_{(CH4)} = 1 - \frac{\mathrm{CH4(Mass\ \%\ in\ the\ plume)}}{\mathrm{CH4\ (Mass\ \%\ in\ the\ original\ fuel)}} \tag{5}$$

Since Methane gas (C1) is the main gas in the flare gas, the DRE has been calculated for Methane gas in the flare. The result of CE% and DRE % are shown in Table 12.

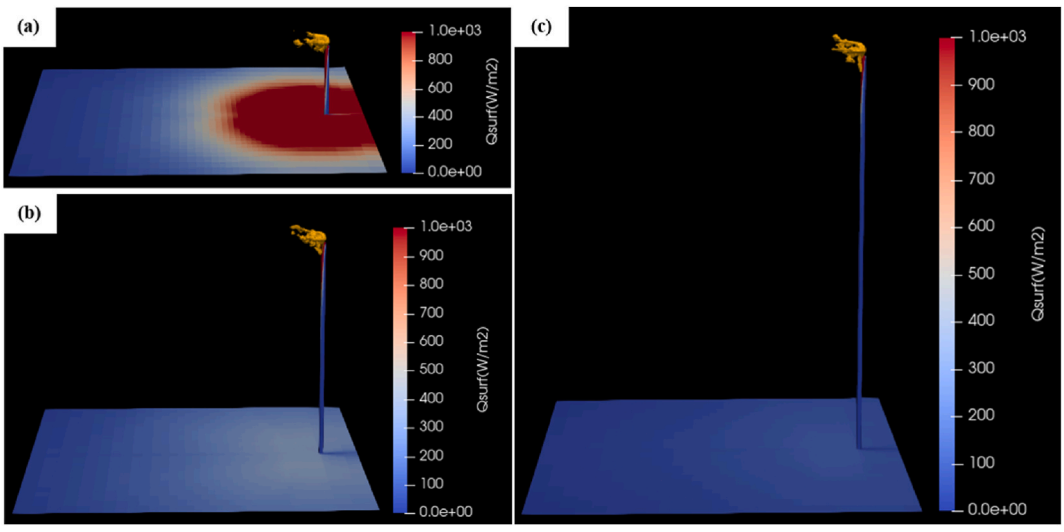

Fig. 18. Stack hieght and ground level heat radiation; (a) 10 m, (b) 30 m, and (c) 50 m

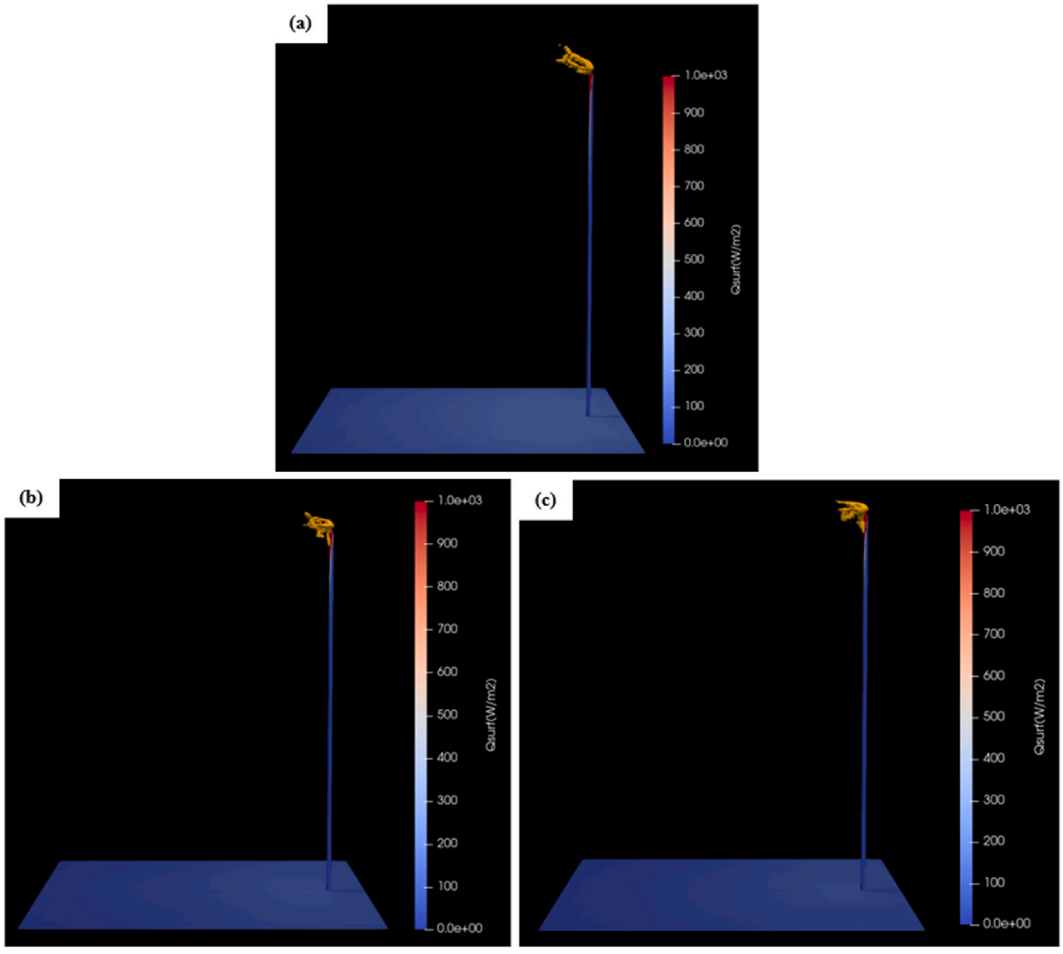

Fig. 19. Cross wind speed and flare flame: (a) 5 m/s, (b) 9 m/s and (c) 14 m/s.

Table 10
Average Temp, CO, CO2, and Soot in the plume at different locations.

Probe				Temp (K)	CO (Mass%)	CO2 (Mass%)	C20 (Mass%)
x-axis	y-axis	z-axis	Radius (m)				
6	0	52	0.25	657.84	7.27E-5	0.033	0.00038
8	0	52	0.25	880.70	8.00E-9	0.121	6.16E-5
10	0	52	0.25	602.16	2.11E-6	0.040	8.71E-5
12	0	52	0.25	490.12	4.53E-6	0.027	0.000109

Table 11
Average C1, C2, C3 and C6+ mass fraction in the plume at three different locations.

Probe				C1 (Mass%)	C2 (Mass%)	C3 (Mass%)	C6+ (Mass%)
x-axis	y-axis	z-axis	Radius (m)				
6	0	52	0.25	7.46E-9	5.39E-9	5.13E-9	4.35E-9
8	0	52	0.25	7.94E-9	7.76E-9	7.60E-9	7.71E-9
10	0	52	0.25	7.46E-9	6.94E-9	6.77E-9	5.94E-9
12	0	52	0.25	5.60E-9	4.85E-9	4.70E-9	4.16E-9

Comparing the results of the fuel distribution in the flame (see Table 11) with fuel concentration in the gas sent to the flare (see Table 2), it's clear that the flare was working perfectly in which all the fuel combusted. For example, the original mass fraction of the methane in the gas sent to the flare is 0.693 and its mass fraction in the plume is around 7.12E-9 (see Table 13). This show that the flare

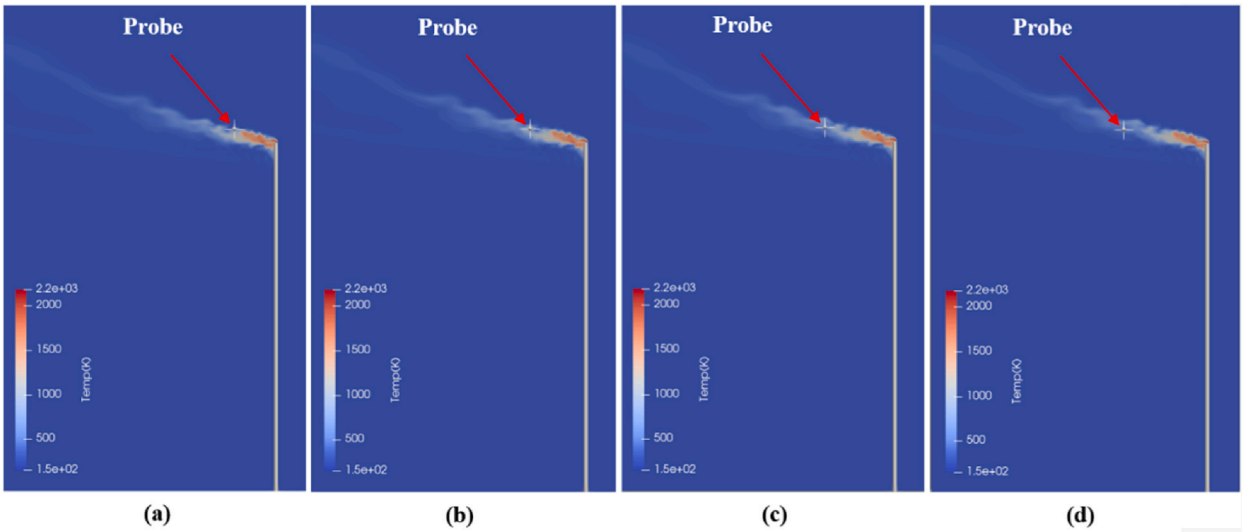

Fig. 20. Probe locations and distance from the stack: (a) 6 m, (b) 8 m, (c) 10 m and (d) 12 m

operation was good and almost all the fuel combusted in the flame. The CE results approve that the flare operation was almost smokeless at least in the area near to the flame. Table 13 show the carbon mass fraction in the flare gas and in the plume for the main carbon compounds in the gas mixture. According to this table, the total carbon mass fraction decreases due to the complete combustion of the gas and good performance of the flare at operation condition.

3.5. Soot formation and combustion efficiency (CE)

The effect of soot formation on flare combustion efficiency has been studied and showed in Table 14. Theoretically, as the soot formation decrease, the CE should increase. According to Table 14, the combustion efficiency increase when the mass % of the soot (C20) decrease. This prove that the flare operation was acceptable and according to requirement.

4. Conclusion

This paper reviewed the design and operation of an oilfield utility flare operating in the Iraq/Kurdistan region. The flare design was carried out using API-521 approach and considering the full firing capacity (100MMSCFD). Results of the design produce a flare with 0.78 m diameter and 48.2 m height, which can be considered reasonable and near to the real flare hydraulic dimensions (50 m high and 0.61 m diameter). Primarily results for flare operation at full capacity showed that as the stack height increases the amount of heat radiation to the ground decreases, and the safest flare height is 133 m with heat radiation 1.6 Kw/m^2 within 45.7 m radius. The CFD code C3d was used to study the flare performance using real flare hydraulic dimensions and depending on real firing rate (1.2 MMSCFD). The results showed that the real flare operation was stable as 1.2 MMSCFD gas firing rate was enough to keep the flame against the applied cross wind of 9 m/s. Moreover, the simulation showed that the real stack height 50 m considered the safety requirement of flare operation with about 150 W/mˆ2 ground heat. The CFD pictures of the flame showed the flame temperature at the center was slightly above 2000 K and decreasing at the shell. Additionally, the CO emissions inside the flame was little and the CO2 was more, which indicate complete combustion and good performance of the flare. Moreover, the soot formation was very low, and the CE calculations proved that with about 98% CE. Furthermore, the DRE calculations showed that the flare has destroyed perfectly all the fuel with 100% DRE. Future prospective of this flare depend of the wind conditions in the region. For example, in the winter, the firing rate should be changed to keep the flame at the tip. Although the flare has very little smoking, air assist can be used to have better smokeless operation.

Table 12
Flare combustion efficiency (CE) and destruction and removal efficiency (DRE).

Probe				CE %	DRE %	DRE $_{(CH4)}$ %
x-axis	y-axis	z-axis	Radius (m)			
6	0	52	0.25	98.7	100	100
8	0	52	0.25	99.9	100	100
10	0	52	0.25	99.8	100	100
12	0	52	0.25	99.6	100	100

Table 13
Carbon balance.

	C1 (Mass%)	C2 (Mass%)	C3 (Mass%)	C6+ (Mass%)	CO_2 (Mass%)	Total Carbon (Mass%)
Carbon Mass % in the flare gas	0.693	0.148	0.078	0.010	0.039	0.968
Average carbon mass % in the plume	7.12E-09	6.24E-09	6.05E-09	5.54E-09	5.53E-02	5.53E-02
						9.13E-01

Table 14
Relation between soot formation and Combution Efficiency (CE).

Probe				C20 (Mass%)	CE %
x-axis	y-axis	z-axis	Radius (m)		
6	0	52	0.25	0.00038	98.7
8	0	52	0.25	6.16E-5	99.9
10	0	52	0.25	8.71E-5	99.8
12	0	52	0.25	0.000109	99.6

Author contribution statement

Ahmed A. Maaroof: Conceived and designed the experiments; Performed the experiments; Wrote the paper.
Joseph D. Smith, Mohammed H.S. Zangana: Analyzed and interpreted the data; Wrote the paper.

Data availability statement

No data was used for the research described in the article.

Declaration of competing interest

The authors declare that they have no known competing financial interests or personal relationships that could have appeared to influence the work reported in this paper.

References

[1] E.A. Emam, Environmental pollution and measurement of gas flaring, Int. J. Innov. Res. Sci. Eng. Technol 2 (2016) 252–262.
[2] A.L. Ling, Flare Selection and Sizing (Engineering Design Guideline), KLM technology group, Malaysia, 2007.
[3] Leslie B. Evans, William M. Vatavuk, Diana K. Stone, Susan K. Lynch, Richard F. Pandullo, VOC Destruction Controls, Office of Air Quality Planning and Standards. U.S Environmental Protection Agency, North Carolina, Durham, 2000.
[4] Natural Gas Sweetening, Natural Gas Processing, 2014, pp. 483–518.
[5] World Bank [Online], https://www.worldbank.org/en/programs/gasflaringreduction/global-flaring-data, 2023.
[6] E.C. Wood, S.C. Herndon, E.C. Fortner, T.B. Onasch, J. Wormhoudt, C.E. Kolb, W.B. Knighton, B.H. Lee, M. Zavala, L. Molina, M. Jones, Combustion and destruction/removal efficiencies of in-use chemical flares in the greater Houston area, Ind. Eng. Chem. Res. 51 (39) (2012) 12685–12696.
[7] Allan, K. C. Combustion Efficiency of Full-Scale Flares Measured Using DIAL Technology. *Alberta Research* Council Inc., *250 Karl Clark Rd.*, Edmonton, Alberta, Canada.
[8] E. Epa, Aug. 2012, Enforcement targets flaring efficiency violations. Enforcement Alert 10 (5) (2012). EPA 325-F-012-002.
[9] M.R. Johnson, O. Zastavniuk, D.J. Wilson, L.W. Kostiuk, Efficiency Measurements of Flares in a Cross Flow, 1999.
[10] M.R. Johnson, A.J. Majeski, D.J. Wilson, L.W. Kostiuk, The Combustion Efficiency of a Propane Jet Diffusion Flame in Cross Flow, Combustion and Environment Group, Department of Mechanical Engineering, University of Alberta, 1998.
[11] D. Joseph, J. Lee, C. McKinnon, R. Payne, J. Pohl, Evaluation of the Efficiency of Industrial Flares: Background- Experimental Design- Facility, 1983.
[12] A. Pederstad, J.D. Smith, R. Jackson, S. Saunier, T. Holm, Assessment of flare strategies, techniques for reduction of flaring and associated emissions, emission factors and methods for determination of emissions to air from flaring, Carbon Limits AS, Trondheim, Norway, 2015 [online] Available from: www.miljødirektoratet.
[13] J.H. Pohl, B.A. Tichenor, J. Lee, R. Payne, Combustion efficiency of flares, Combust. Sci. Technol. 50 (4–6) (1986) 217–231.
[14] J.H. Pohl, N.R. Soelberg, Evaluation of the Efficiency of Industrial Flares: H2S Gas Mixtures and Pilot-Assisted Flares, Energy and Environmental Research Corp., Irvine, CA (USA), 1986. *Final report*, April 1985-July 1986 (No. PB-87-102372/XAB).
[15] J.H. Pohl, N.R. Soelberg, Evaluation of the Efficiency of Industrial Flares: Flare Head Design and Gas Composition, 1985.
[16] API Standard 521. 2012. Guide for Pressure-Relieving and Depressuring Systems. American Petroleum Institute. [Online]. https://www.api.org/~/media/files/publications/whats%20new/521%20e6%20pa.pdf. [Accessed 22/March/2023].
[17] John Zink Company, SAFE FLARE SYSTEM DESIGN, 1993 [Online], https://www.scribd.com/document/61112927/Flare-System. (Accessed 22 September 2022).
[18] J. Seebold, P. Gogoloek, J. Pohl, R. Schwartz, October. Practical implications of prior research on today's outstanding flare emissions questions and a research program to answer them, in: AFRC-JFRC 2004 Joint International Combustion Symposium, Maui, HI, 2004.
[19] L. Aljerf, N. AlMasri, Flame propagation model and combustion phenomena: observations, characteristics, investigations, technical indicators, and mechanisms, Journal of Energy Conservation 1 (1) (2018) 31.
[20] V. Varner, S. Fox, R. Schwartz, R. Wozniak, Pressure-Assisted Flare Emissions Testing, American – Japanese Flame Research Committees International Symposium-Hawaii, 2007.
[21] US Environmental Protection Agency, Parameters for Properly Designed and Operated Flares, 2012 [Online], https://www3.epa.gov/airtoxics/flare/2012flaretechreport.pdf. (Accessed 22 March 2023).

[22] J.D. Smith, A. Suo-Anttila, R. Jackson, S. Smith, Prediction of Plume Formation and Dispersion from Gas Flares, September, Annual American Flame Research Committee Meeting, Salt Lake City, Utah, 2012, pp. 5–7, 2012.
[23] Troy M. B. General Overview of Past and Recent EPA Flare Enforcement Actions (And Flare Assessment Techniques). SAGE Environmental consulting.
[24] J.H. Pohl, R. Payne, J. Lee, Evaluation of the Efficiency of Industrial Flares: Test Results, 1984.
[25] A. Suo-Anttila, C3D Theory and User Manual, 2019.
[26] J.D. Smith, A. Suo-Anttila, S.K. Smith, J. Modi, Evaluation of the Air-Demand, Flame Height, and Radiation Load on the Wind Fence of a Low-Profile Flare Using ISIS-3D". AFRC-JFRC 2007 Joint International Combustion Symposium, October, Marriott Waikoloa Beach Resort Hotel, Hawaii, 2007, pp. 21–24.
[27] J.D. Smith, H.A. Al-Hameedi, R. Jackson, A. Suo-Antilla, Testing and prediction of flare emissions created during transient flare ignition, Int. J. Petrochem. Res 2 (2018) 175–181.
[28] A. Suo-Anttila, K.C. Wagner, M. Greiner, January. Analysis of enclosure fires using the isis-3d™ CFD engineering analysis code, International Conference on Nuclear Engineering 46881 (2004) 721–730.
[29] M. Greiner, N. Are, C. Lopez, A. Suo-Anttila, Effect of small long-duration fires on a spent nuclear fuel transport package, in: Institute of Nuclear Materials Management 45th Annual Meeting, 2004, pp. 18–22.
[30] M. Greiner, A. Suo-Anttila, Radiation heat transfer and reaction chemistry models for risk assessment compatible fire simulations, J. Fire Protect. Eng. 16 (2) (2006) 79–103.
[31] M. Greiner, A. Suo-Anttila, Validation of the Isis-3D computer code for simulating large pool fires under a variety of wind conditions, J. Pressure Vessel Technol. 126 (3) (2004) 360–368.
[32] J.D. Smith, A. Suo-Antilla, S.K. Smith, N. Philpott, Prediction and Measurement of Flare Ignition". American Flame Research Committees-International Pacific Rim Combustion Symposium, Advances in Combustion Technology: Improving the Environment and Energy Efficiency, Sheraton Mavic, 2010. *Hawaii-September 26-29*.
[33] J.D. Smith, R.D. Jackson, A. Suo-Anttila, K. Hefley, Z.D. Smith, D. Wade, S. Smith, Radiation Effects on Surrounding Structures from Multi-point Ground Flares". *AFRC 2015-Industrial Combustion Symposium*, September, Historic Fort Dongles Officer, Club, University of Utah, Salt Lake City, Utah, 2015, pp. 9–11.
[34] J. Smith, B. Adams, R. Jackson, A. Suo-Anttila, Use of RANS and LES Turbulence Models in CFD Predictions for Industrial Gas-fired Combustion Applications, Journal of the International Flame Research Foundation, December, 2017.
[35] Leslie B. Evans, William M. Vatavuk, Diana K. Stone, Susan K. Lynch, Richard F. Pandullo, VOC Destruction Controls, Office of Air Quality Planning and Standards. U.S Environmental Protection Agency, North Carolina, Durham, 2000.
[36] R. Said, A. Garo, R. Borghi, Soot formation modeling for turbulent flames, Combust. Flame 108 (1–2) (1997) 71–86.
[37] A.J. Majeski, D.J. Wilson, L.W. Kostiuk, Size and Trajectory of a Flare in a Cross Flow. Combustion and Environment Group, Department of Mechanical Engineering, May, University of Alberta, Edmonton, Alberta, Canada, T6G 2G8. Presented at Combustion Canada '99, Calgary, Alberta, 1999, pp. 26–28, 1999.
[38] V.M. Torres, S. Herndon, E. Wood, F.M. Al-Fadhli, D.T. Allen, Emissions of nitrogen oxides from flares operating at low flow conditions, Ind. Eng. Chem. Res. 51 (39) (2012) 12600–12605.